Slow dynamics of ablated zone observed around the density fluctuation ridge of fluid medium

Masato Koizumi,[1] Sergei A. Kulinich,[2] Yoshiki Shimizu,[3] and Tsuyohito Ito[1,a)]
[1]*Center for Atomic and Molecular Technologies, Graduate School of Engineering, Osaka University, 2-1 Yamadaoka, Suita, Osaka 565-0871, Japan*
[2]*Institute of Innovative Science and Technology, Tokai University, Hiratsuka, Kanagawa 259-1292, Japan*
[3]*Nanosystem Research Institute, National Institute of Advanced Industrial Science and Technology (AIST), Tsukuba, Ibaraki 305-8565, Japan*

(Received 26 September 2013; accepted 11 November 2013; published online 2 December 2013)

In-situ shadowgraph images were recorded to follow and study processes during laser ablation of Sn targets in pressurized carbon dioxide medium. The dynamics of the low-density region with a bubble-like structure forming by ablated Sn in CO_2 at different pressures was studied. The lifetime of the region is shown to be pressure-dependent, being the longest near the density fluctuation ridge of the medium, i.e., at 8.8 MPa at 40 °C. The present work is to report on the slower dynamics of ablated zone near the medium density fluctuation maximum, which can be used in nanoparticle synthesis and processing. © *2013 AIP Publishing LLC*.
[http://dx.doi.org/10.1063/1.4834517]

Pulsed laser ablation in liquid (LAL) media has currently become a very popular and convenient technique to prepare diverse nanomaterials in laboratory conditions.[1–12] Because of its versatility, low cost, and ease of use, this "green" technique is now extensively studied and applied to prepare various nanostructures such as (but not limited to) nanoparticles (NPs), core-shell NPs, metal-semiconductor heterostructures, nanocubes, layered nanostructures, and hollow NPs.[1–6] A laser beam ablating a solid target can produce plasma from a wide variety of target materials, and therefore NPs with diverse chemistries can be generated depending on the target, laser parameters, and liquid medium.[1–6] The further drastic change in temperature and pressure following the plasma expansion is known to yield highly non-equilibrium processing conditions, which often results in novel nanostructured products with attractive properties.[1–5]

Applying plasmas (including those induced by laser ablation of solid target) to produce novel nanomaterials in supercritical fluids (SCFs) has also attracted much attention lately,[7–10,13,14] as the wide range of physical parameters, from gaseous to liquid-like, achieved with SCF provides additional means to control the product morphology and properties. Up to date, however, the research was mainly focused on nanostructured Si, noble-metal NPs, or carbon-based materials,[8,9,13–17] and only recently on ZnO NPs.[10,18] Plasma generated in a SCF is expected to combine the merits of both "states": the highly reactive environment of plasma and the highly effective and dense transport medium of SCF. Furthermore, under certain conditions, the so-called "clustering" could also be used for processing, so that anomalous reaction rates could be observed near the critical point.[19] Previously, e.g., the "clustering" effect was observed as a rapid change in processing rates near the critical point during Cu film deposition in supercritical CO_2.[11]

The LAL -produced NPs are believed to form following several stages.[1–4] First, a laser pulse heating the target results in the formation of a vapor or plasma plume with vaporized target material. Second, the hot plume transfers a portion of its heat to the target, causing a further vaporization of the target material. Thus, a cavitation bubble is formed and expands after the energy transfer of the plasma plume and its disappearance. During the bubble's expansion and shrinkage (often referred to as "quenching"), with its internal pressure and temperature decreasing, NPs form (and partially) agglomerate.[1–3,6,12] The bubble finally collapses and releases the NPs into the liquid. The ablated vapor region is also often called "bubble." Since in SCFs, as well as in high-pressure gasses, there is no clear bubble (or interphases), hereafter, for convenience, the low-density zone formed by the ablated material near the ablated target is referred to as the bubble-like structure (BLS).

While various NPs have been prepared via laser ablation in pressurized fluid media,[10,13,15,18] their formation and growth are still far from being well understood thus far. The main factors controlling the morphology and chemistry of laser-ablated NPs are known to include laser pulse parameters (pulse duration and energy, frequency and fluence), thermal conductivity and reactivity of the media, and target's chemistry and physical properties.[1–5,14–16] The temporal behavior of the ablated zone (or BLS), which largely influences the growth time of the product, has been scarcely understood, which is partially explained by the lack of experimental data. In this paper, we follow the dynamics of the BLS formed during Sn ablation with a nanosecond pulsed laser in pressurized CO_2. Shadowgraphy experiments performed with a nanosecond time resolution aimed to observe and analyze key stages in the BLS evolution. The results reveal that the lifetime of the BLS is pressure-dependent. Therefore, tuning both experimental pressure and temperature can control the BLS's lifetime, and consequently—the product of the process. The longest lifetime, and hence the

a)E-mail: tsuyohito@ppl.eng.osaka-u.ac.jp

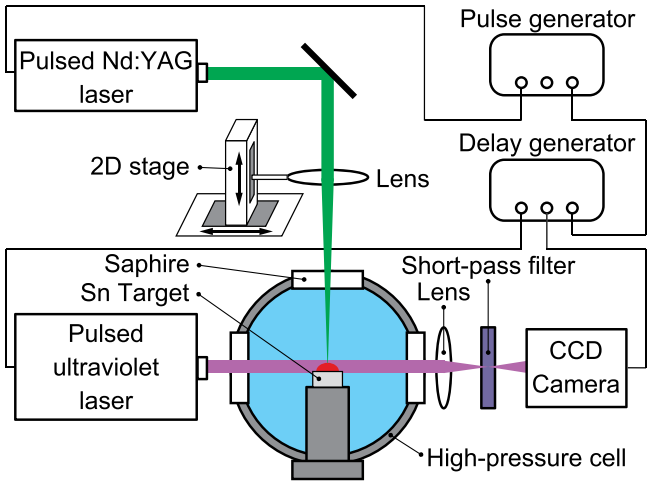

FIG. 1. Experimental set-up used for laser ablation of Sn target and shadowgraph imaging in pressurized CO_2.

longest NP growth time, was observed near the density fluctuation maximum curve of the medium, i.e., at 8.8 MPa (at 40 °C).

In this work, laser ablation in pressurized (including supercritical) CO_2 was studied by means of shadowgraph photography, a technique that has been previously described by several other groups.[11,18,20–23] The experiments were carried out in a high-pressure cell filled with research-grade CO_2 and previously described elsewhere,[14] a schematic diagram of the set-up being presented in Fig. 1. The target material used was Sn rods. The cell is equipped with sapphire windows which are transparent for laser light and can be used for *in-situ* optical investigations during experiments. The second harmonic of a Q-switched pulsed Nd:YAG laser (wavelength 532 nm, pulsed energy 20 mJ, frequency 10 Hz, pulse duration ~5 ns) was applied. The laser beam was focused on the Sn target by using a lens with a 10 cm focal length. The cell temperature was maintained at 40 °C, while the pressure of the system was varied from 0.1 to 14.5 MPa. The critical point of carbon dioxide is 31 °C and 7.38 MPa.[19]

The shadowgraph images of the ablated zone were taken with a nanosecond resolution by using another Nd:YAG laser operating with the third harmonic (i.e., 355 nm) and with a duration time of approximately 5 ns. The time delay between the two pulsed lasers was controlled with a delay generator. The light of the imaging laser was passing through the ablation zone, projecting shadowgraphs on a CCD camera. The imaging laser beam was parallel to the target surface and normal to the ablating beam (see Fig. 1). The CCD camera had a short-pass filter cutting off 532 nm light, so that any light scattered from the ablating beam was not affecting the images. No signals were recorded by the CCD camera when the imaging laser was off. To avoid any disturbance or light scattering caused by previously ablated craters, the ablating laser beam was shifted, and thus intact Sn surface was always ablated.

Another series of experiments was carried out to analyze the ablated product and evaluate the target ablation rate. While the experimental conditions were same, the irradiation time was 50 min. Silicon wafers located in the cell during experiments were used to collect NPs. The NPs were then analyzed with X-ray diffractometry (XRD) and transmission electron microscopy (TEM). The weight reduction rate of the target was evaluated as the difference between the target weight before and after each experiment.

Figure 2 presents typical examples of shadowgraph images taken at different medium pressures (5.0, 8.8, and 14.3 MPa) and with delay times of 0.5 (a1–c1), 3.0 (a2–c2), 5.0 (a3–c3), 10.0 (a4–c4), and 20 μs (a5–c5). Based on the images in Fig. 2, the evolution of the BLS can be described in four distinct phases, which are presented schematically in Fig. 3. The first phase is the BLS formation caused by a laser pulse heating the target. Within the whole range of tested

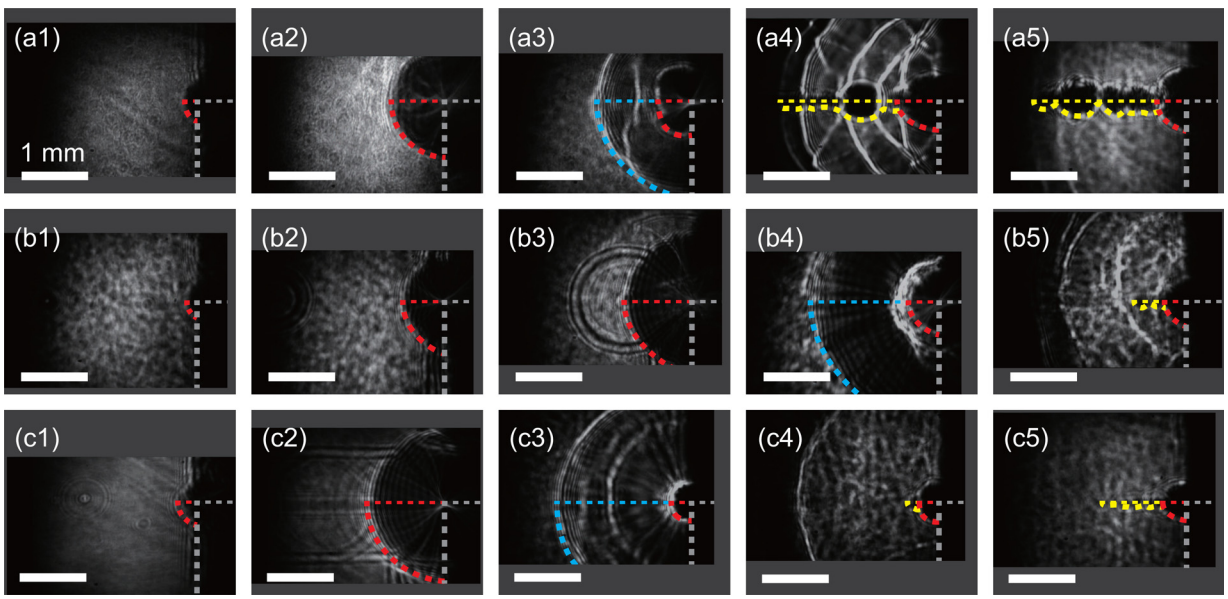

FIG. 2. Time-resolved shadowgraph images of the laser-induced "bubble" formed on target surface at different medium pressures: (a1 ~ a5) 5.0 MPa, (b1–b5) 8.8 MPa, and (c1–c5) 14.3 MPa. Delay times are: 0.5 (1), 3.0 (2), 5.0 (3), 10.0 (4), and 20 μs (5). The white scale bar indicates 1 mm. The broken lines indicate: BLS edge with shockwave front in phase 2 (red); shockwave front in phase 3 (blue); nanoparticles dissipating into the medium (yellow); and Sn target (gray).

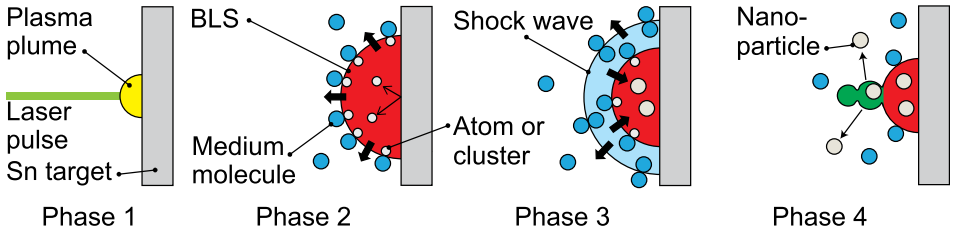

FIG. 3. Four phases of the ablated zone evolution observed in shadowgraph images.

conditions, dark semispherical BLSs were found to form within ~500 ns after the laser pulse impact on the target surface (Figs. 2(a1)–2(c1)). The BLS observed in Figs. 2(a1)–2(c1)) was believed to be Sn vapor ablated from the Sn target.[1,2,4,24] The initiation of the BLS, (i.e., phase 1) could not be clearly detected at the spatial resolution (being ~6.2 μm/pixel) used in this experiment, and therefore in this study we focused primarily on the further phases of the BLS evolution (phases 2 to 4 in Fig. 3). In the second phase, the BLS was expanding (Figs. 2(a2)–2(c2)). During this stage, no separation of the BLS from the shockwave was observed. The third phase was associated with the BLS shrinkage, implying that the BLS reached its maximum size between phases 2 and 3 (see Fig. 3). In phase 3, a clear separation of the shrinking BLS from the still-expanding shockwave (indicated by dashed blue lines in Fig. 2) was observed for the low-pressure cases ($\leq$7.7 MPa), while the BLS could not be seen inside the shockwave at higher pressure ($\geq$8.8 MPa) during the initial stage of phase 3 (discussed below). Finally, during phase 4, the BLS disintegrated from its tip, releasing Sn species from the ablated zone (indicated with dashed yellow lines in Fig. 2), which might be the product NPs dissipating into the surrounding medium.

Figure 4 displays the evolution of the above phases 2–4 over time as a function of medium pressure. Also shown is the size ratio of the BLS to its separated shockwave at the time when phase 3 was first observed in shadowgraph images. The solid blue squares indicate the transition from phase 3 to phase 4 as observed in the shadowgraph experiments, and hence the time for the most intense release of product materials into the medium. The solid red circles mark the time when the separation between the BLS and the shockwave was first clearly seen in the shadowgraph images, thus implying the BLS shrinkage in phase 3 (see, e.g., Fig. 2(b4)). For comparison, the solid black triangles present theoretical values for the phase 2 to phase 3 transition obtained by applying the Rayleigh's theory[25] (that describes the shrinkage of a cavitation bubble in a liquid, see details below). At lower pressures ($\leq$7.7 MPa), the solid red circles and the solid black triangles agree very well, since the separation of the BLS and shockwave could be well resolved from a semi-initial stage of phase 3 (indicated by the BSL to shockwave size ratio values close to 1). However, at pressures equal or over 8.8 MPa, a significant difference between the two lines is seen in Fig. 4. Thus, there is a large uncertainty about the phase 2 to phase 3 transition time at higher pressures ($\geq$8.8 MPa): while the upper limit of phase 2 might be indicated with the line with solid red circles, the lower limit of phase 3 might be marked with the line with solid black triangles. This large uncertainty can be attributed to the difficulties with the BLS observation inside the shockwave as darker and less clear images were recorded at higher pressures. As seen in Figs. 2(b) and 2(c), the entire images were found to become darker at higher pressures. In addition, the BLS edges often appeared somewhat distorted (see, e.g., Fig. 2(b4)), probably because of the non-uniform density of the medium. Therefore, while at lower pressures (Fig. 2(a3)) the BLS could be clearly seen inside the shockwave with a similar radius (implying the beginning of phase 3), at higher pressures the resolved BLS was typically much smaller than the size of the shockwave, like in Figs. 2(b4) and 2(c3), which is also demonstrated by the line with red open diamonds in Fig. 4.

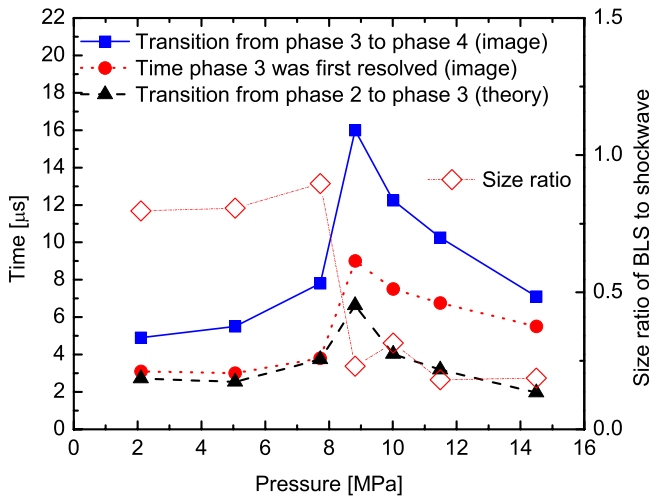

FIG. 4. Evolution of phases 2–4 over time as a function of CO_2 medium pressure at 40 °C (solid symbols) and the size ratio of BLS to shockwave front at the time phase 3 was first resolved in shadowgraph images (open red diamonds). Solid blue squares: transition from phase 3 to phase 4 observed in shadowgraph images. Solid red circles: time when phase 3 was first resolved in shadowgraph images. Solid black triangles: theoretical time when BLS reaches its maximum (transition from phase 2 to phase 3 begins).

Interestingly, at 8.8 MPa the duration of phases 2 and 3 is seen in Fig. 4 to be the longest. This is also seen in Fig. 2 as panels b2–b5 present earlier BLS phases observed after 5.0 and 10.0 μs when compared to those in panels a2–a5 and c2–c5. This implies that the dynamics (both expansion and shrinkage) of the BLS were the slowest near this pressure. This also means that all processes associated with the product formation took longer time near 8.8 MPa, which should influence the products (as discussed below). Note that the value of 8.8 MPa corresponds to the pressure with the largest density fluctuation at 40 °C.[19]

The time t_3 that takes a cavitation bubble to shrink in a liquid with density ρ, at liquid pressure P and vapor saturation pressure P_{vap} from a maximum radius R_0 to a radius R_1,

according to the Rayleigh's theory,[25] can be described by the following formula:

$$t_3 = \sqrt{\frac{3}{2}\frac{\rho}{(P - P_{vap})}}\int_{R_1}^{R_0} \frac{R^{3/2}}{(R_0{}^3 - R^3)^{1/2}}\,dR.$$

We applied this formula to estimate the phase 2 to phase 3 transition times shown with the broken black line in Fig. 4, even though the medium was not liquid but a pressurized gas or SCF. To use the above formula, we assumed that in phase 2 the BLS was expanding along with its shockwave, i.e., the R_0 at the beginning of phase 3 coincided with the size of shockwave at the phase 2 to phase 3 transition. Another assumption was a negligibly small internal pressure of the BLS (P_{vap}) compared to that of the medium pressure, which should be reasonable during the shrinkage stage. Since R_1 could be estimated from the solid blue line in Fig. 4 (as the time when the BLS shrank and started dissipating), the shrinkage time t_3 (presented by the broken black line in Fig. 4) could be found. Also found in the analysis was the maximum size R_0, which is the largest near 8.8 MPa. Table I shows the values used for and extracted from the above described calculations. The applied theoretical approach thus gives results that are consistent with the experimental observations and also indicates the existence of size maximum at 8.8 MPa. The shrinkage time t_3, which is seen as the difference between the blue and black lines in Fig. 4, is also the longest near this pressure. In the high-pressure region ($\geq$ 8.8 MPa), the theory suggests that the maximum BLS size is smaller and its shrinkage time is also smaller. This agrees with the smaller sizes of the "cavitation bubble" previously observed for Ti laser-ablated in pressurized water.[20]

Figure 5 shows the weight reduction rate of the target as a function of medium pressure at 40 °C. At lower pressures, the plasma plume was relatively large[10,20] and the energy density on the target surface was smaller, thus resulting in smaller ablation rates of the target. With an increase in pressure, the shrunk and denser plasma (or the BLS) should transfer more energy into the Sn target, and therefore a larger amount of Sn vapor should be ablated and dissipated to the surrounding medium. Thus the weight reduction rate should generally increase with pressure. However, interestingly, a local minimum is clearly observed around 8.8 MPa, which is associated with the slowest BLS dynamics described above. We attribute this local minimum to re-deposition of ablated

TABLE. I Values used for theoretical calculations using (and extracted from) the Rayleigh's formula.

Pressure [MPa]	Speed of shockwave [m/s]	R_1 [mm]	R_0 [mm]	t_3 [μs]
2.1	315	0.66	0.86	2.2
5.1	315	0.44	0.80	2.9
7.7	243	0.48	0.91	4.1
8.8	233	0.46	1.55	9.4
10.0	304	0.44	1.23	8.2
11.5	348	0.51	1.11	7.1
14.5	441	0.39	0.86	5.1

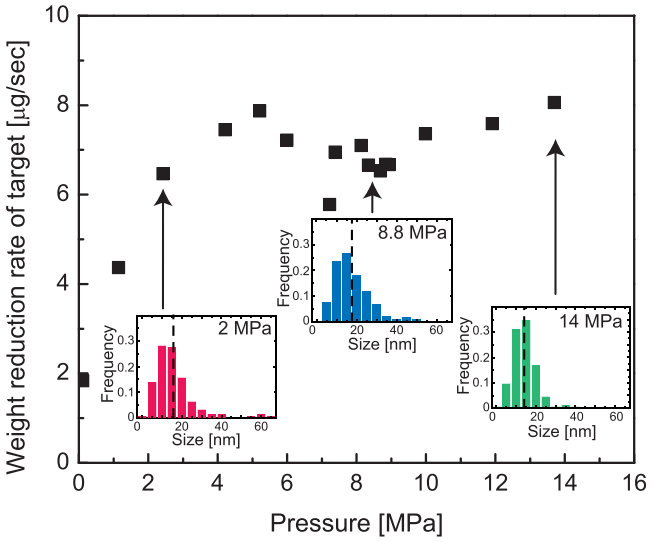

FIG. 5. Weight reduction rate of Sn target as a function of CO_2 medium pressure at 40 °C. Insets are size distribution histograms for nanoparticles prepared at 2.0 MPa, 8.8 MPa, and 14.0 MPa. The broken lines in the insets indicate average diameters observed by TEM.

Sn species onto the target, as the ablated BLS had the longest lifetime at this pressure. This assumption is supported by the fact that a small bump surrounding the crater was found on the surface of the target ablated at 8.8 MPa, which was not observed at higher and lower pressures.

The produced NPs were characterized by XRD and TEM. The XRD patterns from different samples were almost identical, implying no detectable pressure effect as all the samples were indexed as tetragonal Sn. The prepared NPs were thus composed of metallic Sn with no any detectable amount of oxide phases. As seen in Fig. 5 (insets), TEM analysis revealed that most of the NPs were 10–30 nm in size. However, while the average sizes were centered at ~17.5 nm for the NPs prepared at 2.0 and 8.7 MPa, their counterparts prepared at 8.8 MPa were centered at ~19.0 nm, thus being slightly bigger. The sizes of the NPs prepared at 12.0 and 14.0 MPa were centered at ~17.5 and ~15.0 nm, respectively, thus tending to be smaller at higher pressures. Hence, both the weight reduction rate and the NP size distribution show a local minimum or maximum around 8.8 MPa, where the BLS lifetime was found to be the longest. It is reasonable to assume that the long lifetime of the BLS around 8.8 MPa resulted in both more re-deposition and more intense agglomeration during the NP formation and growth.[26]

This study thus demonstrates that by adjusting the medium conditions, it is possible to use the lifetime of the BLS (or ablated zone) as one of parameters. This value exhibits a maximum around the pressure with density fluctuation maximum. The BLS lifetime has an impact on the product NPs, as their size distribution changes. This effect can be more profound in the systems where chemical reactions are also involved during NP formation, and therefore needs to be studied more carefully in the future.

The work was carried out with the financial support from the Japan Society for the Promotion of Science (JSPS),

as well as from the Iketani Science and Technology Foundation. S.A.K. acknowledges the support from the Ministry of Education, Culture, Sports, Science and Technology of Japan. Encouragements from Prof. S. Okada (Osaka Univ.) are also greatly appreciated.

[1]H. B. Zeng, X. W. Du, S. C. Singh, S. A. Kulinich, S. K. Yang, J. P. He, and W. P. Cai, Adv. Funct. Mater. **22**, 1333 (2012).
[2]V. Amendola and M. Meneghetti, Phys. Chem. Chem. Phys. **15**, 3027 (2013).
[3]Z. J. Yan and D. B. Chrisey, J. Photochem. Photobiol. C **13**, 204 (2012).
[4]K. Y. Niu, J. Yang, S. A. Kulinich, J. Sun, H. Li, and X. W. Du, J. Am. Chem. Soc. **132**, 9814 (2010).
[5]K. Y. Niu, J. Yang, S. A. Kulinich, J. Sun, and X. W. Du, Langmuir **26**, 16652 (2010).
[6]W. J. Qin, S. A. Kulinich, X. B. Yang, J. Sun, and X. W. Du, J. Appl. Phys. **106**, 114318 (2009).
[7]T. Ito, K. Katahira, Y. Shimizu, T. Sasaki, N. Koshizaki, and K. Terashima, J. Mater. Chem. **14**, 1513 (2004).
[8]S. Nakahara, S. Stauss, H. Miyazoe, T. Shizuno, M. Suzuki, H. Kataoka, T. Sasaki, and K. Terashima, Appl. Phys. Express **3**, 096201 (2010).
[9]S. Nakahara, S. Stauss, T. Kato, T. Sasaki, and K. Terashima, J. Appl. Phys. **109**, 123304 (2011).
[10]S. A. Kulinich, T. Kondo, Y. Shimizu, and T. Ito, J. Appl. Phys. **113**, 033509 (2013).
[11]T. Kato, S. Stauss, S. Kato, K. Urabe, M. Baba, T. Suemoto, and K. Terashima, Appl. Phys. Lett. **101**, 224103 (2012).
[12]A. De Giacomo, M. Dell'Aglio, A. Santagata, R. Gaudiuso, O. De Pascale, P. Wagener, G. C. Messina, G. Compagnini, and S. Barcikowski, Phys. Chem. Chem. Phys. **15**, 3083 (2013).
[13]K. Saitow, T. Yamamura, and T. Minami, J. Phys. Chem. C **112**, 18340 (2008).
[14]T. Ito and T. Tamura, Chem. Phys. Lett. **502**, 173 (2011).
[15]S. Wei and T. Yamamura, J. Phys. Chem. C **116**, 3928 (2012).
[16]S. Machmudah, Y. Kuwahara, M. Sasaki, and M. Goto, J. Supercrit. Fluids **60**, 63 (2011).
[17]Y. Kuwahara, T. Saito, M. Haba, T. Iwanaga, M. Sakaki, and M. Goto, Jpn. J. Appl. Phys., Part 1 **48**, 040207 (2009).
[18]W. Soliman, N. Takada, N. Koshizaki, and K. Sasaki, Appl. Phys. A **110**, 779 (2013).
[19]R. Span and W. Wagner, J. Phys. Chem. Ref. Data **25**, 1509 (1996).
[20]K. Sasaki, T. Nakano, W. Soliman, and N. Takada, Appl. Phys. Express **2**, 046501 (2009).
[21]W. Soliman, N. Takada, and K. Sasaki, Appl. Phys. Express **3**, 035201 (2010).
[22]M. Tiberi, A. Simonelli, G. Cristoforetti, P. Marsili, F. Giammanco, and E. Giorgetti, Appl. Phys. A **110**, 857 (2013).
[23]E. Popov, M. Mammetkuliyev, and J. Eloranta, J. Chem. Phys. **138**, 204307 (2013).
[24]R. E. Treece, J. S. Horwitz, and J. H. Claassen, Appl. Phys. Lett. **65**, 2860 (1994).
[25]H. Lindgren and E. Bjarne, "In connection with the modern development of merchant ships," in *Proceedings of Conference on Cavitation, IME, Heriot-Watt University*, 1974.
[26]S. Ibrahimkutty, P. Wagener, A. Menzel, A. Plech, and S. Barcikowski, Appl. Phys. Lett. **101**, 103104 (2012).